JOURNAL OF ENVIRONMENTAL SCIENCES 150 (2025) 556–570

Available online at www.sciencedirect.com

ScienceDirect

www.elsevier.com/locate/jes

JES JOURNAL OF ENVIRONMENTAL SCIENCES

www.jesc.ac.cn

Effects of isoprene on the ozonolysis of Δ^3-carene and β-caryophyllene: Mechanisms of secondary organic aerosol formation and cross-dimerization

Zhaoyan Zhang[1,2], *Yingqi Zhao*[1,2], *Ya Zhao*[1], *Xiangyu Zang*[1], *Hua Xie*[1], *Jiayue Yang*[1], *Weiqing Zhang*[1], *Guorong Wu*[1], *Gang Li*[1,*], *Xueming Yang*[1,3,4], *Ling Jiang*[1,3,*]

[1] *State Key Laboratory of Molecular Reaction Dynamics, Dalian Institute of Chemical Physics, Chinese Academy of Sciences, Dalian 116023, China*

[2] *University of Chinese Academy of Sciences, Beijing 100049, China*

[3] *Hefei National Laboratory, Hefei 230088, China*

[4] *Department of Chemistry and Guangdong Provincial Key Laboratory of Catalytic Chemistry, Southern University of Science and Technology, Shenzhen 518055, China*

ARTICLE INFO

Article history:
Received 31 July 2023
Revised 21 November 2023
Accepted 21 November 2023
Available online 29 November 2023

Keywords:
Secondary organic aerosol
Δ^3-Carene and β-caryophyllene
Ozonolysis
Cross reaction
Isoprene

ABSTRACT

Elucidating the mutual effects between the different volatile organic compounds (VOCs) is crucial for comprehending the formation mechanism of atmospheric secondary organic aerosols (SOA). Here, the mixed VOCs experiments of isoprene and Δ^3-carene/β-caryophyllene were carried out in the presence of O_3 using an indoor smog chamber. The suppression effect of isoprene was recognized by the scanning mobility particle sizer spectrometer, online vacuum ultraviolet free electron laser (VUV-FEL) photoionization aerosol mass spectrometry, and quantum chemical calculations. The results indicate that the suppression effect of isoprene on the ozonolysis of Δ^3-carene and β-caryophyllene shows fluctuating and monotonous trends, respectively. The carbon content of the precursor could be the main factor for regulating the strength of the suppression effect. Plausible structures and formation mechanisms of several new products generated from the single VOC precursor and VOC-cross-reaction are proposed, which enrich the category of VOC oxidation products. Meanwhile, a new dimerization mechanism of the $RO_2 + R'O_2$ reaction is suggested, which offers an intriguing perspective on the gas phase formation process of particle phase accretion products. The present findings provide valuable insights into clarifying the pivotal roles played by isoprene in the interplay between different VOCs and understanding of SOA formation mechanisms of VOC mixtures, especially nearby the emission origins.

* Corresponding authors.
E-mails: gli@dicp.ac.cn (G. Li), ljiang@dicp.ac.cn (L. Jiang).

https://doi.org/10.1016/j.jes.2023.11.024
1001-0742/

Introduction

Secondary organic aerosol (SOA) generated from the oxidation of biological volatile organic compounds (BVOCs) is a crucial source of fine particles, which seriously affects the balance of atmospheric radiation, traffic safety, and human health (Brauer et al., 2016; Ehn et al., 2014; Hallquist et al., 2009; Lewis, 2018; Shiraiwa et al., 2017). Terpenoids represent an important class of BVOCs. Laboratory studies and field measurements of terpenoids (i.e., hemiterpenes, monoterpenes, and sesquiterpenes) have provided important insights into the atmospheric fate of BVOCs (Atkinson and Arey, 2003; Guenther et al., 2012; Koch et al., 2000; Liu et al., 2016; Wennberg et al., 2018; Winterhalter et al., 2009). Currently, numerous studies mainly focus on understanding the impacts of anthropogenic pollutants (i.e., O_3, NO_x, and SO_2) on the oxidation of single-component VOCs and the corresponding mechanisms (Atkinson, 2000; Kleindienst et al., 2006; Shrivastava et al., 2019; Xu et al., 2015). However, the SOA formation is known to be intricately affected by the types and concentrations of VOCs and oxidants, owing to the complexity of precursors in the ambient atmosphere. The studies on the multi-component VOCs have thus emerged in recent years, highlighting the requirements for more detailed experiments of mixed VOCs to provide a more scientific basis for reducing pollution and carbon emissions (Ahlberg et al., 2017; Heinritzi et al., 2020; McFiggans et al., 2019; Takeuchi et al., 2022).

The investigation of the SOA formation from a mixture system containing various monoterpenes and sesquiterpenes revealed a pronounced enhancement in SOA mass concentration as compared to a single-component monoterpene system, implying that the simplification of terpene complexity in SOA models might underpredict the aerosol mass loading (Faiola et al., 2018). The SOA production of anthropogenic VOCs (AVOCs) was found to be enhanced (+83.9%) by the coexistence with other AVOCs but suppressed (-51.4%) by the presence of isoprene through OH scavenging (Chen et al., 2022). Suppression effects of isoprene have even been observed in areas where monoterpenes are abundant (Kanawade et al., 2011; Lee et al., 2016; Li et al., 2022; Wimmer et al., 2018). A smog chamber study of α-pinene showed that the SOA formation was monotonically suppressed by increasing the mixing ratio of isoprene, suggesting that isoprene not only plays the role of OH scavenger, but also removes the monoterpene-derived highly oxidized products with low volatility (McFiggans et al., 2019). Recent investigation indicated that the rapid reaction of isoprene with OH promotes the formation of isoprene-derived RO_2 rather than the C_{20} products, ultimately affecting particle nucleation (Heinritzi et al., 2020).

In the multi-component VOCs system, an assumption implemented in the simulation of SOA mass concentrations is that SOA is formed independently from each individual VOC precursor (Appel et al., 2017). However, a study on mixed AVOCs indicated that the interaction between intermediate products is the primary factor contributing to the improvement in SOA mass concentrations as compared to single precursor conditions (Li et al., 2021). The particle-phase accretion products generated from the ozonolysis of the monoterpene mixture were tentatively identified by liquid chromatography-mass spectrometry, but the specific formation pathway was not clear (Thomsen et al., 2022). Previous studies have put forth various hypotheses of the dimer formation, including the connection of two monomers in the form of ester or anhydride (Hamilton et al., 2006; Mueller et al., 2008; Yasmeen et al., 2010), oligomer formation in atmospheric organic aerosols through acid- or base-catalyzed heterogeneous reactions (Gao et al., 2004; Tolocka et al., 2004), and dimerization between peroxyl radicals (RO_2) in the gas phase (Hasan et al., 2021, 2020; Salo et al., 2022). During the oxidation of VOCs, reaction intermediates containing different functional groups are generated, including organic acids that have a significant contribution in the SOA formation (Zhang, 2010; Zhang et al., 2004). However, the process of condensing organic acids with other products to create dimer products in the gas phase requires strict reaction conditions. Chen et al. (2022) pointed out that the cross-reaction of RO_2 produced by different AVOCs is the main source of SOA formation (up to 39.0%), emphasizing the importance of the $RO_2 + R'O_2$ reaction in the case of mixed VOCs. Recent study of multiple BVOCs mixtures also highlighted the importance of RO_2 cross-reactions in the formation of highly oxygenated dimers (Dada et al., 2023).

In contrast with α-pinene, Δ^3-carene ($C_{10}H_{16}$) possesses a different geometrical structure with a three-membered ring (Scheme 1) (Ma et al., 2009; Yu et al., 1999). This raises an interesting issue: what is the difference in the isoprene effect on the ozonolysis of Δ^3-carene and α-pinene? β-caryophyllene ($C_{15}H_{24}$) (Scheme 1) exhibits higher reactivity with O_3 in comparison to isoprene and monoterpene (Ciccioli et al., 1999; Ng et al., 2007), and can even dominate the SOA formation depending on the region and season (Geron and Arnts, 2010). Does the addition of isoprene also have a suppression effect on the ozonolysis of β-caryophyllene (Heinritzi et al., 2020)? Based on the previous hypothesis (Heinritzi et al., 2020), would the C_5 and C_{15} products readily react to form the C_{20} cross-products to promote the new particles formation? In order to clarify these aforementioned issues, this study conducted the mixed VOC experiments using isoprene in combination with Δ^3-carene and β-caryophyllene. We analyzed the potential impact mechanisms of isoprene on the ozonolysis of Δ^3-carene and β-caryophyllene by examining the changes in particles under different mixing conditions. The plausible structures and formation pathways for newly-observed single-precursor products and double-precursor cross-products in particle phase were proposed with the combination of online

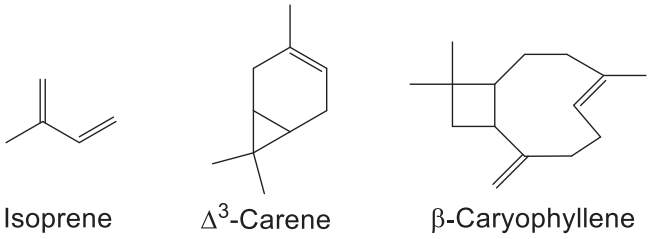

Scheme 1 – Structures of isoprene, Δ^3-carene, and β-caryophyllene.

vacuum ultraviolet free electron laser (VUV-FEL) photoionization mass spectrometry and theoretical calculations. These results shed light on the suppression effect of isoprene on the SOA formation of monoterpenes and sesquiterpenes in areas with abundant vegetation and high levels of O_3 pollution. This work affords a novel pathway for the cross-dimerization of ester accretion products through the RO_2 reaction, potentially leading to the formation of a large variety of other types of accretion complexes.

1. Methods

1.1. Experimental methods

The experiments involved in this study were carried out in an indoor smog chamber (DICP-Chamber) with a built-in cylindrical Teflon reactor with a volume of 2 m^3, and the detailed descriptions have been reported in a previous study (Zang et al., 2022). Before each experiment, the reactor was purged with zero gas for at least 12 hr. The smog chamber was operated in a static mode. The relative humidity (RH) in the reaction chamber was < 2.0%, and the temperature was 23.2 ± 1.3°C. The liquid phase of isoprene (99.0%, Aladdin), Δ^3-carene (90.0%, Aladdin), and β-caryophyllene (90.0%, Innochem) was introduced into the reactor by zero air at 40°C. A dual-channel injection was used for two-precursor experiments. Gas phase and particle phase species were characterized by various instruments. The VOCs were characterized by proton-transfer reaction mass spectrometer (PTR-QMS 3500, East & West Analytical Instruments, China). The concentration of O_3 was measured by a gas analyzer (Model 49i, Thermo Fisher Scientific, UK). The number concentrations and size distributions of particles were measured by a scanning mobility particle sizer spectrometer (SMPS 3938NL76, TSI Incorporated, USA).

The chemical compositions of the particles were detected by a home-built aerosol time-of-flight mass spectrometer (TOF-MS) based on VUV-FEL photoionization (Zang et al., 2022). The VUV-FEL mass spectrometer can detect particle-phase products online. A silicone tubing (inner diameter size: 6.35 mm; length: 1 m) was used to connect the reaction chamber and the TOF-MS chamber coupled to the VUV-FEL beamline. The measurement range of aerosol size for the home-built aerosol MS was 30–2500 nm, which covered the main size distribution of the particles. Considering that the VUV-FEL beamline time is very expensive and the reaction time of VOCs with O_3 is shorter at high concentrations than that at low concentrations, the VUV-FEL photoionization mass spectra of the compounds were thus measured at higher concentrations of isoprene, Δ^3-carene, β-caryophyllene, and O_3 than the atmospheric conditions. The optimum experimental conditions were found by carefully optimizing the reactant concentrations to be closer to the atmospheric levels and the wavelength and pulse energy of VUV-FEL to avoid the saturation of photoionization. In order to compare the impact of the mixing amount of isoprene on the experimental results, low- and high-isoprene conditions were set respectively by ensuring that the mass spectrum of the particle components could be detected.

The SOA yield was the ratio of ΔM and ΔROG (ΔM: the mass concentration of formed SOA; ΔROG: the amount of reacted organic gas). During the experiments in the smog chamber, some particles were lost to the wall, resulting in a decrease in the particle mass concentrations. Assuming that the wall loss rate was first order and that the loss rate constant was independent of size (Pathak et al., 2007). The rate constant k for the loss of aerosol mass to the wall was given by:

$$\ln[(M(t)] = -kt + C \quad (1)$$

where, C is a constant. A plot of ln[M(t)] versus time after the cessation of SOA generation provided the mass loss rate constant k (hr^{-1}) as the slope of the corresponding line. The fitting calculation obtains k. SOA(t) was given by:

$$SOA(t) = M(t) + k\int_0^t M(t)dt - M_S \quad (2)$$

where, M_S is the seed concentration at the time when the SOA formation begins. All reactions were carried out under seed-free aerosol conditions. Taking the 100 ppb Δ^3-carene + 45 ppb isoprene + 100 ppb O_3 experiment as an example, temporal profiles for wall-loss corrected and uncorrected SOA number concentrations and mass concentrations are shown in Appendix A Fig. S1a and b, respectively. In the calculation of SOA yield, the value of SOA mass concentration was corrected. The losses of organic vapor included gas-particle loss and gas-wall loss. The gas-particle loss of organic vapor led to the particle growth. However, precise evaluation of the gas-wall losses of organic vapor in a smog chamber with nucleation event is very challenging (Krechmer et al., 2020; Zhang et al., 2014). Therefore, the loss of organic vapor was not taken into consideration in this study. For the O_3-only experiments in this study, it was assumed that all O_3 reacted directly with VOCs, so we assumed that all uncertainty on the aerosol mass yield was due to the precision of the ΔM measurement. Uncertainty in ΔM estimated by replicating measurements of 100 ppb Δ^3-carene + 45 ppb isoprene + 100 ppb O_3 was < 14.0% (Appendix A Fig. S1c).

1.2. Theoretical methods

Geometric optimization and frequency calculations of the intermediates, transition states, and products involved in the whole pathways were performed using the Gaussian 16 program package (Frisch et al., 2016) at the M06–2X/def2-TZVP level of theory. Based on the optimized structures, single-point energy calculations were carried out at the ωB97XD/aug-cc-pVTZ level of theory. The relative energies included the zero-point energy (ZPE) corrections. In the discussion of cross-products, the most stable isomers of RO, ^{3}(RO…OR'), ^{3}(RO…R'), $^3CP_{HC}$, and $^1CP_{HC}$ generated from the mixed VOC systems were determined by regularly rotating the target angles using the Molclus program (Lu, 2023). The structure of R was determined according to the most stable structure of RO after CO_2 dissociation. The detailed screening process is described in the Appendix A. Based on the transition state structures for the dissociation of CO_2 by RO(i), RO(Δ), and RO(β) (i stands for isoprene, Δ for Δ^3-carene, and β for β-caryophyllene,

Table 1 – Overview of the experimental conditions.

$[isoprene]_0$ (ppmV)	HC_1 $[\Delta^3\text{-carene}]_0$ (ppmV)	HC_2 $[\beta\text{-caryophyllene}]_0$ (ppmV)	$[O_3]_0$ (ppbV)	$\Delta ROG_{isoprene}/\Delta ROG_{HC}$ (μg/μg)	ΔM (μg/m^3)	SOA yield
0	3.7	–	304	0	2083	30.9%
0.6	3.7	–	289	0.18	2144	19.5%
1.7	3.7	–	290	0.41	2377	13.6%
0	–	3.7	1451	0	3887	12.5%
0.6	–	3.7	1488	0.10	2629	14.1%
1.7	–	3.7	1493	0.29	1454	6.4%

$[X]_0$: the initial concentration of the species X; ΔROG: the amount of reacted organic gas; ΔM: the mass concentration of formed SOA.

respectively) optimized by the Berny algorithm, the multi-conformers searches were also performed through freezing the atoms relevant to chemical reactions using the Molclus program, but no other target conformers were found. The reaction rate constants for the dissociation of CO_2 by RO(i), RO(Δ), and RO(β) were calculated using the variational transition state theory (VTST) (Bao and Truhlar, 2017) with the KiSThelP program (Canneaux et al., 2014).

2. Results and discussion

In this work, the mixed VOCs experiments of isoprene with Δ^3-carene (referred as HC_1) or β-caryophyllene (HC_2) were conducted in the presence of O_3. The experimental conditions are listed in Table 1. The effect of initial concentration of isoprene on the particle number concentration and mass concentration of SOA formed from the ozonolysis of Δ^3-carene and β-caryophyllene was evaluated in combination with the reaction rate of precursors with oxidant. The plausible structures and formation pathways of the newly observed single-precursor products and VOC-cross-product dimers were analyzed on the basis of VUV-FEL photoionization mass spectra and quantum chemical calculations.

2.1. *Effects of isoprene on the number concentration and mass concentration of SOA generated from the ozonolysis of Δ^3-carene and β-caryophyllene*

The particle size distribution and mass concentration as a function of initial concentration of isoprene are shown in Fig. 1. For the isoprene + Δ^3-carene experiments, when the initial concentration of isoprene varied from 0.0 to 0.6 ppmV, the particle number concentrations decrease significantly (Fig. 1a), indicative of a pronounced suppression effect of isoprene; the particle size at maximum number concentration increases slightly from 120 to 130 nm, which may be due to the easy adsorption of isoprene oxidation products on the surface of the Δ^3-carene-derived particles. Although the particle number concentration is significantly reduced, the particle mass concentration is virtually unchanged with the variation of isoprene concentration from 0.0 to 0.6 ppmV (Fig. 1c), indicating that the particle mass concentration is compensated by the isoprene-derived products. When the initial concentration of isoprene increases to 1.7 ppmV, the particle size also increases slightly to 140 nm; the maximum number concentration is remarkably higher than that at the condition with isoprene concentration of 0.6 ppmV; the particle mass concentration is even higher than that at the condition without isoprene mixing. This indicated that the suppression effect of isoprene on the reaction of Δ^3-carene with O_3 is weakened with isoprene concentration of 1.7 ppmV. In other words, as the mixing amount of isoprene increases, the interphase interaction between isoprene- and Δ^3-carene-derived intermediates is enhanced, resulting in a compensation in the particle mass concentration. These experimental phenomena indicate that as the mixing amount of isoprene increases, the suppression effect on the ozonolysis of Δ^3-carene is not monotonically changed but fluctuated, which are different from the monotonous effect of isoprene on the reaction of α-pinene with OH (McFiggans et al., 2019). Such difference might be mainly due to the different molecular structures of Δ^3-carene and α-pinene.

To further understand the difference in the effect of isoprene on the SOA formation of Δ^3-carene and α-pinene, we did a comparative experiment at low concentrations similar to the literature (McFiggans et al., 2019). The experimental conditions are listed in Appendix A Table S1. The particle mass concentrations as a function of the ratio ($\Delta ROG_{isoprene}/\Delta ROG_{\Delta^3\text{-carene}}$) is shown in Appendix A Fig. S2. In the range of ratio 0–6.53, the suppression effect of isoprene on particle mass concentration shows a fluctuation trend with increasing the ratio (Appendix A Fig. S2a), which is similar to the experimental results under high concentrations. This may be due to the gradual increase in the proportion of the isoprene oxidation. The SOA yields also fluctuate with the ratio (Appendix A Fig. S2b).

For the isoprene + β-caryophyllene experiments, when the mixing amount of isoprene increases from 0.6 to 1.7 ppmV, the suppression effect of isoprene is observed for both particle number concentration and mass concentration (Fig. 1b and **d**), which are different from the isoprene + Δ^3-carene experiments (Fig. 1a and **c**); the particle size at the maximum number concentration increased from 85 to 126 nm, indicating that increasing the concentration of isoprene has a significant competitive effect on O_3, but its products maybe more likely adsorb on the surface of particles generated by β-caryophyllene to increase the particle size, rather than nu-

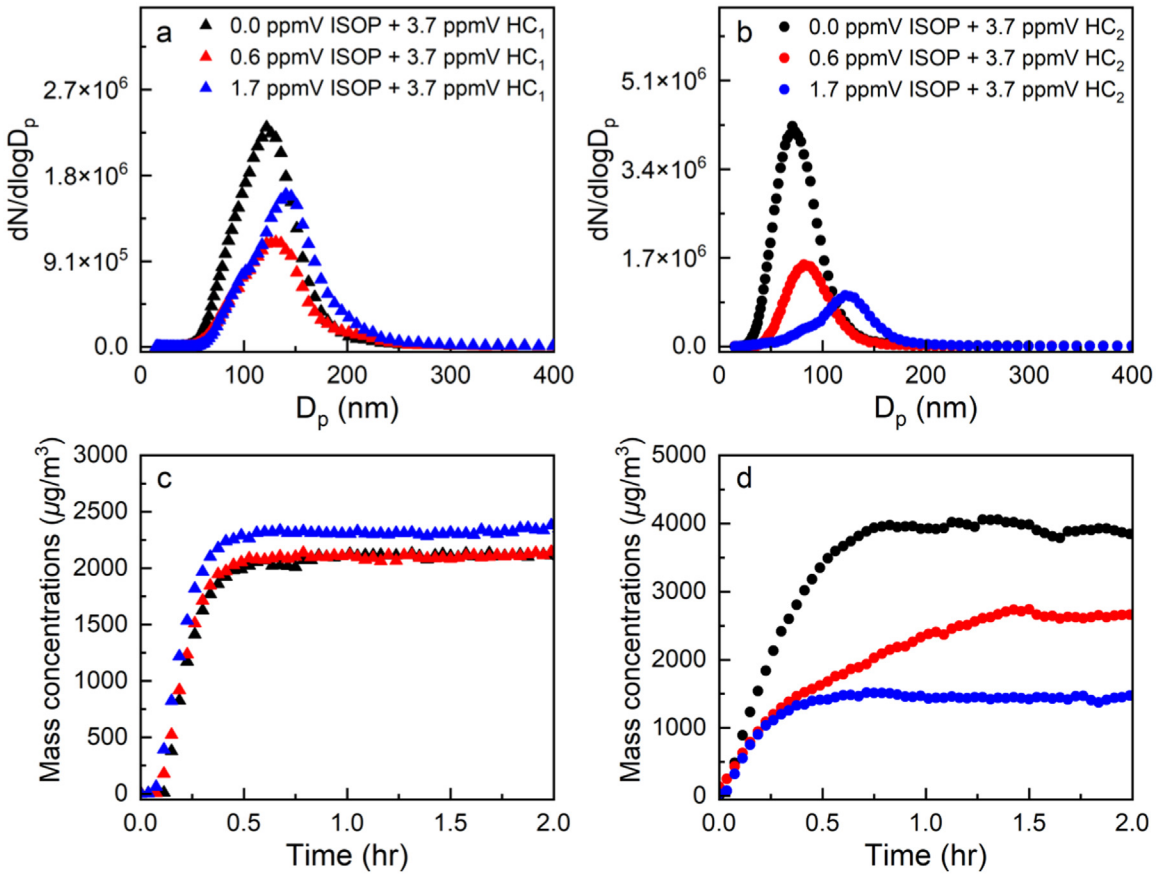

Fig. 1 – Particle size distributions at maximum number concentrations (a and b) and SOA mass concentrations (c and d) as a function of the amount initial concentration of isoprene. ISOP, HC_1, and HC_2 represents isoprene, Δ^3-carene, and β-caryophyllene, respectively. D_p: particle diameter; $dN/dlogD_p$: normalized number size distribution.

cleate to form particles. The monotonous suppression effect of isoprene on the ozonolysis of β-caryophyllene is similar to previous findings (McFiggans et al., 2019).

The mechanism for suppression effect of isoprene on the ozonolysis of Δ^3-carene and β-caryophyllene is proposed as follows. The reaction rate constant and lifetime for the reaction of BVOCs with O_3 and OH are listed in Appendix A Table S2 (Atkinson and Arey, 2003; Bonn and Moortgat, 2002; Hantschke et al., 2021; Winterhalter et al., 2009; Zhang et al., 2002, 2000). In the conditions of Δ^3-carene + isoprene, the reaction rate constant of Δ^3-carene and O_3 is approximately three times higher than that of isoprene and O_3 ($k_{\Delta 3\text{-carene}} = 4.4 \times 10^{-17}$ cm^3/(molecule*sec), $k_{isoprene} = 1.6 \times 10^{-17}$ cm^3/(molecule*sec)). Since the concentrations of Δ^3-carene is higher than that of isoprene in this study, the ozonolysis of Δ^3-carene is dominant. At the stage when the increase in the amount of isoprene weakens the suppression effect on the Δ^3-carene ozonolysis, the difference in the concentrations between Δ^3-carene and isoprene might facilitate the production of C_{15} dimers (formed from the cross-intermediate reaction of Δ^3-carene and isoprene) with lower volatility, which in turn promotes the SOA formation. However, as the amount of isoprene continues to increase, the entire reaction is gradually dominated by the isoprene ozonolysis. Though this promotes the production of C_5 complexes (derived from the isoprene oxidation), it is not favorable for particle nucleation because of higher volatility of C_5 complexes. Ultimately, the suppression effect of isoprene on the ozonolysis of Δ^3-carene shows fluctuating trend. However, in the mixed reaction of α-pinene and isoprene, the suppression effect of isoprene on the oxidation of α-pinene shows monotonous trend (McFiggans et al., 2019). The different suppression effect of isoprene on the SOA formation of two monoterpene is due to the different structures of precursors. The three-membered carbocycle of Δ^3-carene has stronger tension than the four-membered carbocycle of α-pinene, which makes Δ^3-carene more reactive and unstable. In addition, the secondary oxidant (OH) could be generated from the VOC oxidation (Fuchs et al., 2014; Lester and Klippenstein, 2018; Zhang and Zhang, 2002), and it might also be one of the factors for regulating the strength of suppression effect. However, the specific mechanism is difficult to elucidate in this study.

In the condition of β-caryophyllene + isoprene, the reaction rate constant of β-caryophyllene and O_3 is nearly 3 orders of magnitude higher than that of isoprene and O_3 ($k_{\beta\text{-caryophyllene}} = 1.2 \times 10^{-14}$ cm^3/(molecule*sec) (endocyclic), $k_{isoprene} = 1.6 \times 10^{-17}$ cm^3/(molecule*sec)). With the increase of isoprene concentration, the competition of isoprene for O_3 is more significant, leading to a reduction in the number of C_{15} products and intermediates. While the C_{15} in-

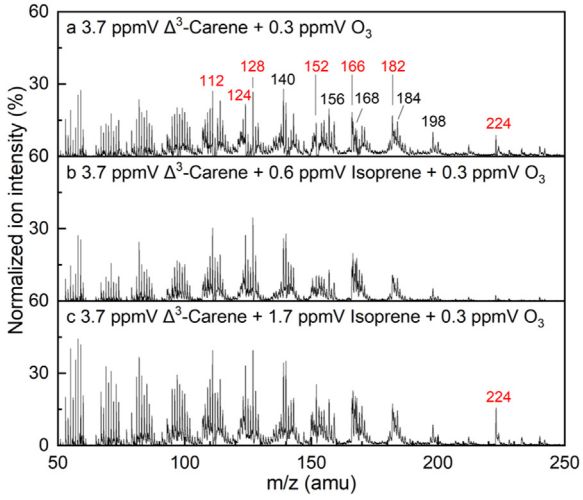

Fig. 2 – VUV-FEL photoionization mass spectra of the compounds generated from the ozonolysis of Δ^3-carene under different concentrations of isoprene. The compounds were ionized by the VUV-FEL at 118.0 nm. The newly-observed peaks are marked in red.

termediates play a key role in the formation of lower volatile products. Thus, the number of C_{20} accretion products formed from the C_{15} + C_5 cross reactions decrease with the decrease of C_{15} intermediates. In contrast with the Δ^3-carene experiments, the more obvious suppression phenomenon in the β-caryophyllene ozonolysis reflects the importance of C_{15} products and intermediates in the SOA formation. As reported by Dada et al. (2023), the addition of sesquiterpenes in the mixed reaction of isoprene and α-pinene increases the yield of ultralow-volatility organic compounds (ULVOC) and promotes the SOA formation.

2.2. VUV-FEL photoionization mass spectra of SOA

In this study, mass spectra of particle components were detected continuously from the time of particle observed. The intensities of overall mass spectral peaks gradually increased as the particles formation and growth, and gradually decreased as the particles sedimentation. Taking the ozonolysis of Δ^3-carene and β-caryophyllene as the examples, the temporal profiles for the intensities of newly-observed peaks are shown in Appendix A Fig. S3 and S4, respectively. During the continuous detection, there was no significant change in the positions of mass peaks. Relative ion intensities (m/z > 100) normalized by SOA mass concentrations in the Δ^3-carene + isoprene and β-caryophyllene + isoprene experiments are illustrated in Appendix A Fig. S5 and S6, respectively.

2.2.1. Mass spectral analysis of the effects of isoprene on the ozonolysis of Δ^3-carene

Fig. 2 shows the photoionization mass spectra of the compounds generated from the ozonolysis of Δ^3-carene under different concentrations of isoprene. Upon the addition of 0.6 ppmV isoprene (Fig. 2b), the intensity of the product peak m/z = 224 decreases notably. This decrease could be attributed to the competition between the reactions of isoprene + O_3 and Δ^3-carene + O_3 that reduces the proportion of products derived from Δ^3-carene, implying that the contribution of VOC-cross product is not substantial. However, after adding 1.7 ppmV isoprene, the intensity of the *m*/z = 224 peak increases significantly, along with an overall increase in the intensity of other product peaks. This is likely due to the formation of cross products from ozonolysis of the Δ^3-carene and isoprene mixture. Therefore, two different components might be involved in the m/z = 224 product. In Fig. 2b, the intensities of the m/z = 152, 156, 182, 184, and 198 peaks decrease significantly, indicative of the pronounced suppression effect of isoprene. It can be seen from Appendix A Fig. S5 that the intensities of the m/z = 156, 182, 184, and 198 peaks under the condition of 3.7 ppmV Δ^3-carene + 1.7 ppmV isoprene + 0.3 ppmV O_3 decreased slightly as compared to the condition of 3.7 ppmV Δ^3-carene + 0.3 ppmV O_3, but increase obviously as compared to the condition of 3.7 ppmV Δ^3-carene + 0.6 ppmV isoprene + 0.3 ppmV O_3. The increase in the proportion of these products in the particle phase may be due to both the formation of VOC-cross products and the increase in mass concentration and particle size. Among them, the relative intensity of the m/z = 152 peak changes obviously, indicating that the change of isoprene concentration has a remarkable effect on the m/z = 152 compound. The peak intensity of m/z = 168 increases in both conditions with isoprene, which may be mainly stemmed from the oxidation of isoprene or/and the formation of VOC-cross products. The corresponding structure of m/z = 168 in the ozonolysis of isoprene has been pointed out in previous studies (2-hydroxy-dihydroperoxide ($C_5H_{12}O_6$)) (Amaladhasan et al., 2022).

The m/z = 112, 124, 128, and 140 compounds account for a relatively high proportion in the product peaks, and their intensities increase with the concentration of isoprene, which may be due to the formation of VOC-cross products or the increase of particle size. The overall intensities of the 50 < *m*/z < 100 peaks decrease slightly in Fig. 2b and increase obviously in Fig. 2c. These signals may be originated from the cleavage of intermediate products, and are clearly related to the changes of particle size, number concentration, and mass concentration. When the particle number concentration decreases significantly and the mass concentration remains basically unchanged in the 3.7 ppmV Δ^3-carene + 0.6 ppmV isoprene + 0.3 ppmV O_3 experiment (Fig. 2b), the intensities of the 50 < m/z < 100 peaks decrease relative to Fig. 2a. Such trend holds true for the *m*/z = 140, 152, 156, 182, 184, 198, and 224 peaks, indicating that the mutual polymerization between these products has a significant impact on the nucleation of particulate matter. When the particle number concentration decreases and the mass concentration increases (Fig. 2c, 3.7 ppmV Δ^3-carene + 1.7 ppmV isoprene + 0.3 ppmV O_3), the intensities of the 50 < m/z < 100 peaks increase relative to the condition of 3.7 ppmV Δ^3-carene + 0.3 ppmV O_3. Such trend holds true for the m/z = 140 and 152 peaks, illustrating that these products may be readily adsorbed by particles.

To understand the structures and formation mechanisms of ozonolysis products (100 < m/z < 250) of Δ^3-carene, we performed quantum chemical calculations. The product is labeled as $\mathbf{P_{HC1}}$-$\boldsymbol{n}$ (n = 1–12) sorted by the molecular weight,

and the intermediate is successively labeled as $\mathbf{I_{HC1}}$-***m*** (*m* = 1–11). The structures of the m/z = 140 (Yu et al., 1999), 156 (Yu et al., 1998), 168 (Ma et al., 2009), 184 (Ma et al., 2009), and 198 (Koch et al., 2000) products have been proposed in the previous studies, and the m/z = 112, 124, 128, 152, 166, 182, and 224 products are the newly-observed species in this work, which benefit from the advantages of high-efficiency ionization of VUV-FEL. Newly-observed products identified in the ozonolysis of Δ^3-carene are listed in Appendix A Table S3. We will mainly analyze these newly-observed products, for which the corresponding molecular weights are marked in red in Figs. 2-7. The formation pathways of $\mathbf{P_{HC1}}$**–1** (m/z = 224) and $\mathbf{P_{HC1}}$**–6** (m/z = 166) are proposed in Fig. 3. O_3 is added to the double bond of Δ^3-carene to form a primary ozonide (**POZ**), which is a high-energy unstable substance (marked with *) and undergoes a rapid ring-opening reaction to produce $\mathbf{I_{HC1}}$**–1.** $\mathbf{P_{HC1}}$**–5** (m/z = 168) (3-caronaldehyde) is formed by the $O(^3P)$ radical elimination reaction of $\mathbf{I_{HC1}}$**–1**, which is calculated to be exothermic by 20.3 kcal/mol. The hydrogen on the -CH_2- and aldehyde groups in $\mathbf{P_{HC1}}$**–5** is abstracted by OH to produce $\mathbf{I_{HC1}}$**–2** and $\mathbf{I_{HC1}}$**–3**, respectively, with an exothermic value of 32.5 and 29.1 kcal/mol and the energy of the transition state relative to the $\mathbf{P_{HC1}}$**–5** + OH complex of -0.3 and -4.5 kcal/mol, respectively. $\mathbf{P_{HC1}}$**–6** (m/z = 166) is generated by the H-abstraction from $\mathbf{I_{HC1}}$**–2** with a transition state energy of -3.8 kcal/mol relative to the reactants. $\mathbf{I_{HC1}}$**–5** is obtained by multi-step reactions from $\mathbf{I_{HC1}}$**–3**, during which the energy barrier for the dissociation of CO and CH_2O is 13.7 and 19.7 kcal/mol, respectively. $\mathbf{I_{HC1}}$**–5** and $\mathbf{I_{HC1}}$**–6** (the formation process of $\mathbf{I_{HC1}}$**–6** could be referred to $\mathbf{I_{HC1}}$**–13** in Fig. 4) react with each other to form accretion products $\mathbf{P_{HC1}}$**–1** (m/z = 224) (Perakyla et al., 2023), which process is calculated to be highly exothermic by 70.6 kcal/mol.

The reaction pathways of $\mathbf{P_{HC1}}$-***n*** **(*n* = 4, 7, 8, 10, 11, 12)** are shown in Fig. 4. $\mathbf{P_{HC1}}$**–3** (m/z = 184) stemmed from the unstable **POZ** could undergo a H-abstraction reaction to produce $\mathbf{I_{HC1}}$**–7**, which is exothermic 29.3 kcal/mol, and the relative energy of the transition state relative to the reactant is -3.9 kcal/mol. $\mathbf{I_{HC1}}$**–7** undergoes an intramolecular hydrogen shift isomerization (H-shift) to produce $\mathbf{I_{HC1}}$**–8** with a barrier of 16.4 kcal/mol. $\mathbf{P_{HC1}}$**–4** (m/z = 182) is obtained by the H-abstraction reaction from $\mathbf{I_{HC1}}$**–8**, for which the $\mathbf{I_{HC1}}$**–7** → $\mathbf{P_{HC1}}$**–4** process is calculated to be exothermic by 65.0 kcal/mol. $\mathbf{I_{HC1}}$**–7** releases CO to produce $\mathbf{I_{HC1}}$**–9**, which is endothermic by 9.0 kcal/mol with a barrier of 13.5 kcal/mol. A new structure of $\mathbf{P_{HC1}}$**–7′** (m/z = 156) is formed by the hydrogenation of $\mathbf{I_{HC1}}$**–9.** $\mathbf{P_{HC1}}$**–3** can readily release CH_2OH to produce $\mathbf{I_{HC1}}$**–10** prior to its own stabilization (Yu et al., 1998). $\mathbf{I_{HC1}}$**–10** undergoes an intramolecular H-shift to form $\mathbf{I_{HC1}}$**–11** with a barrier of 14.6 kcal/mol, and the subsequent H-abstraction reaction produces $\mathbf{P_{HC1}}$**–8** (m/z = 152), for which the $\mathbf{I_{HC1}}$**–10** → $\mathbf{P_{HC1}}$**–8** process is calculated to be highly exothermic by 67.0 kcal/mol. $\mathbf{I_{HC1}}$**–10** could also release CO to produce $\mathbf{I_{HC1}}$**–12**, which is slightly endothermic by 7.9 kcal/mol with a barrier of 12.8 kcal/mol. $\mathbf{I_{HC1}}$**–12** undergoes an intramolecular H-shift (on the aldehyde) with a barrier of 13.5 kcal/mol and proceeds the dissociation of CO with a barrier of 13.5 kcal/mol and the bimolecular reaction with RO_2, resulting in the formation of $\mathbf{I_{HC1}}$**–13**, for which the $\mathbf{I_{HC1}}$**–12** → $\mathbf{I_{HC1}}$**–13** process is exothermic by 38.2 kcal/mol. The hydrogen atom on the -CH_2- of $\mathbf{I_{HC1}}$**–13** is extracted by O_2 to form $\mathbf{P_{HC1}}$**–12** (m/z = 112), for which the process is exothermic 31.6 kcal/mol and the relative energy of its transition state relative to the reactant is 12.5 kcal/mol. $\mathbf{P_{HC1}}$**–10** (m/z = 128) is obtained from $\mathbf{P_{HC1}}$**–12** after multi-step reactions. $\mathbf{I_{HC1}}$**–12** could also undergo dehydrogenation reaction to form $\mathbf{P_{HC1}}$**–11** (m/z = 124) and analogues including $\mathbf{P_{HC1}}$**–4** and $\mathbf{P_{HC1}}$**–8**. These products containing unsaturated double bonds are readily formed in this hypothesis and can participate in the ozonolysis again.

2.2.2. *Mass spectral analysis of the effects of isoprene on the ozonolysis of β-caryophyllene*

Fig. 5 shows the VUV-FEL photoionization mass spectra of the compounds generated from the ozonolysis of β-caryophyllene under different concentrations of isoprene. As the mixing amount of isoprene increases, the suppression effect becomes more apparent and the overall trend of the mass spectrum peaks decreases. Upon the addition of 0.6 ppmV isoprene (Fig. 5b), the peak intensity of the m/z = 126, 152, and 198 products increase notably as compared to the absence of isoprene, whereas those of other products are significantly weakened besides m/z = 168 and 182 products. Upon the addition of 1.7 ppmV isoprene (Fig. 5c), the m/z = 198 peak is still observed, whereas other peaks in the range of m/z = 50–250 are barely detected. It is speculated that the m/z = 198 peak may contain multiple components. Under the mixed-VOC conditions, the origin of the m/z = 198 peak is mainly attributed to the formation of VOC-cross products, which may compensate for its peak intensity observed in Fig. 5b. In Fig. 5, it is found that after adding 0.6 ppmV isoprene (Fig. 5b), the relative intensities of some product peaks in the range of m/z = 50–250 change as compared to the absence of isoprene (Fig. 5a). The variation in the relative intensity of the m/z = 166 and 168 peaks may be due to the oxidation product of isoprene (Amaladhasan et al., 2022), or to the compensation by the VOC-cross product. The intensity of the m/z = 128 peak is noticeably lower than that of m/z = 126. It is hypothesized that the primary source of m/z = 128 is the ozonolysis product of β-caryophyllene.

Quantum chemical calculations were carried out to understand the structures and formation mechanisms of ozonolysis products ($100 < m/z < 250$) of β-caryophyllene. The nomenclature for ozonolysis products of β-caryophyllene is similar to that of Δ^3-carene. The structures of the *m*/z = 238, 224 (Atkinson and Arey, 2003), 198, 166, 152, 140, 126, and 112 (Du et al., 2023) products have been proposed in the previous studies, for which the formation pathways are given in Appendix A Fig. S7. Here, we focus on the analyses of the newly-observed products of m/z = 128, 168, 182, and 214. Newly-observed products identified in the ozonolysis of β-caryophyllene are listed in Appendix A Table S4. The structures and formation pathways of $\mathbf{P_{HC2}}$-***n*** (*n* = 3, 5, 6, 10) are shown in Fig. 6. After the hydrogen on the aldehyde group of $\mathbf{P_{HC2}}$**–2** (m/z = 224) is extracted by OH, the RO_2 radical obtained by autoxidation reacts with other RO_2 intermolecularly to produce alkoxyl radicals (RO), and ultimately releases the CHO group to form $\mathbf{I_{HC2}}$**–1**, for which the $\mathbf{P_{HC2}}$**–2** → $\mathbf{I_{HC2}}$**–1** process is exothermic by 49.9 kcal/mol with a small dissociation energy barrier of 8.7 kcal/mol. $\mathbf{I_{HC2}}$**–1** undergoes H-abstraction reaction and releases CO to form $\mathbf{I_{HC2}}$**–2**, which overall pro-

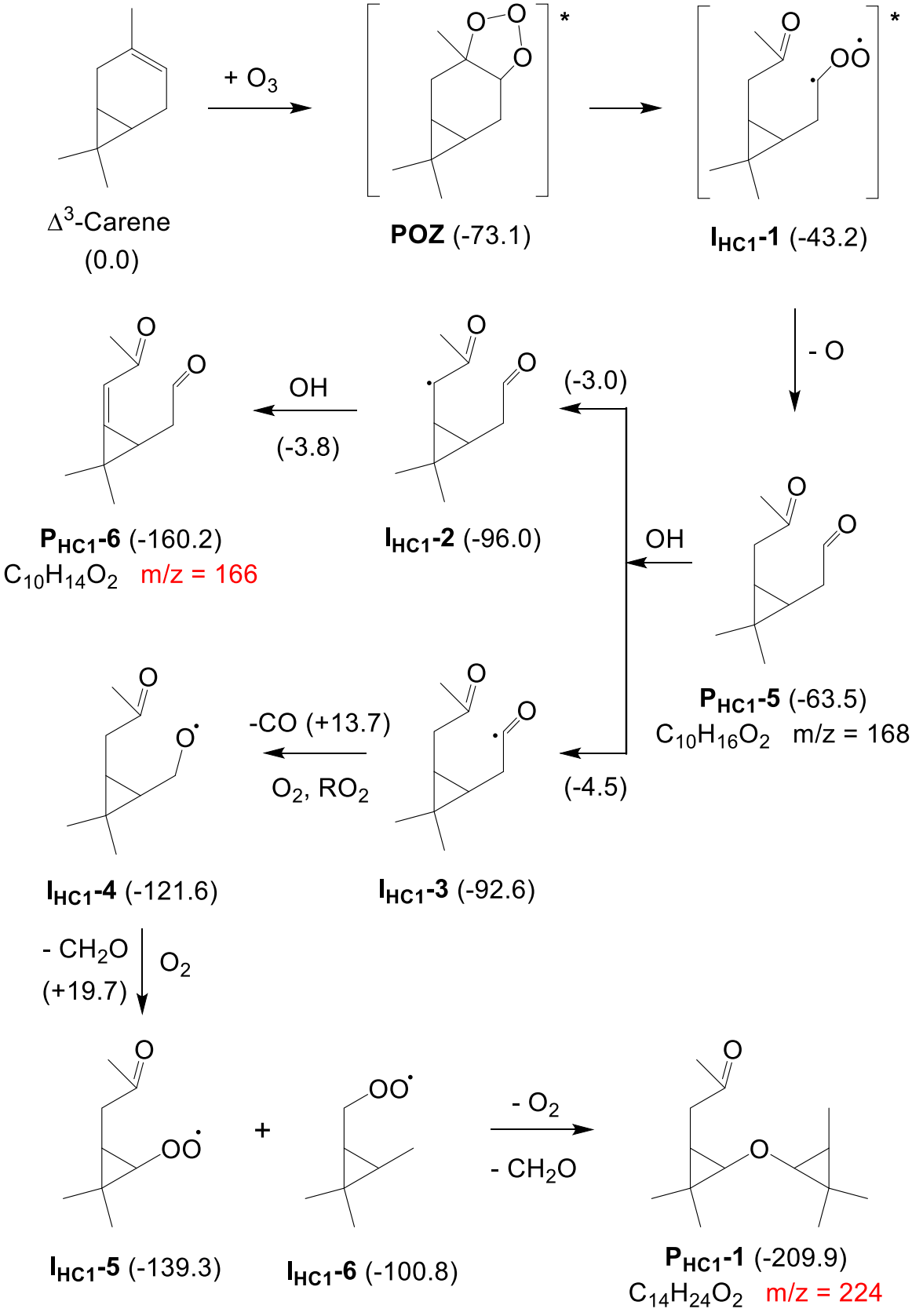

Fig. 3 – Possible formation mechanisms of newly-observed species P_{HC1}–1 and P_{HC1}–6 generated from the ozonolysis of Δ^3-carene calculated at the ωB97XD/aug-cc-pVTZ//M06–2X/def2-TZVP level of theory. Relative energies are given in kcal/mol. The values in parentheses beside the arrows are the relative energies of transition states and reactants.

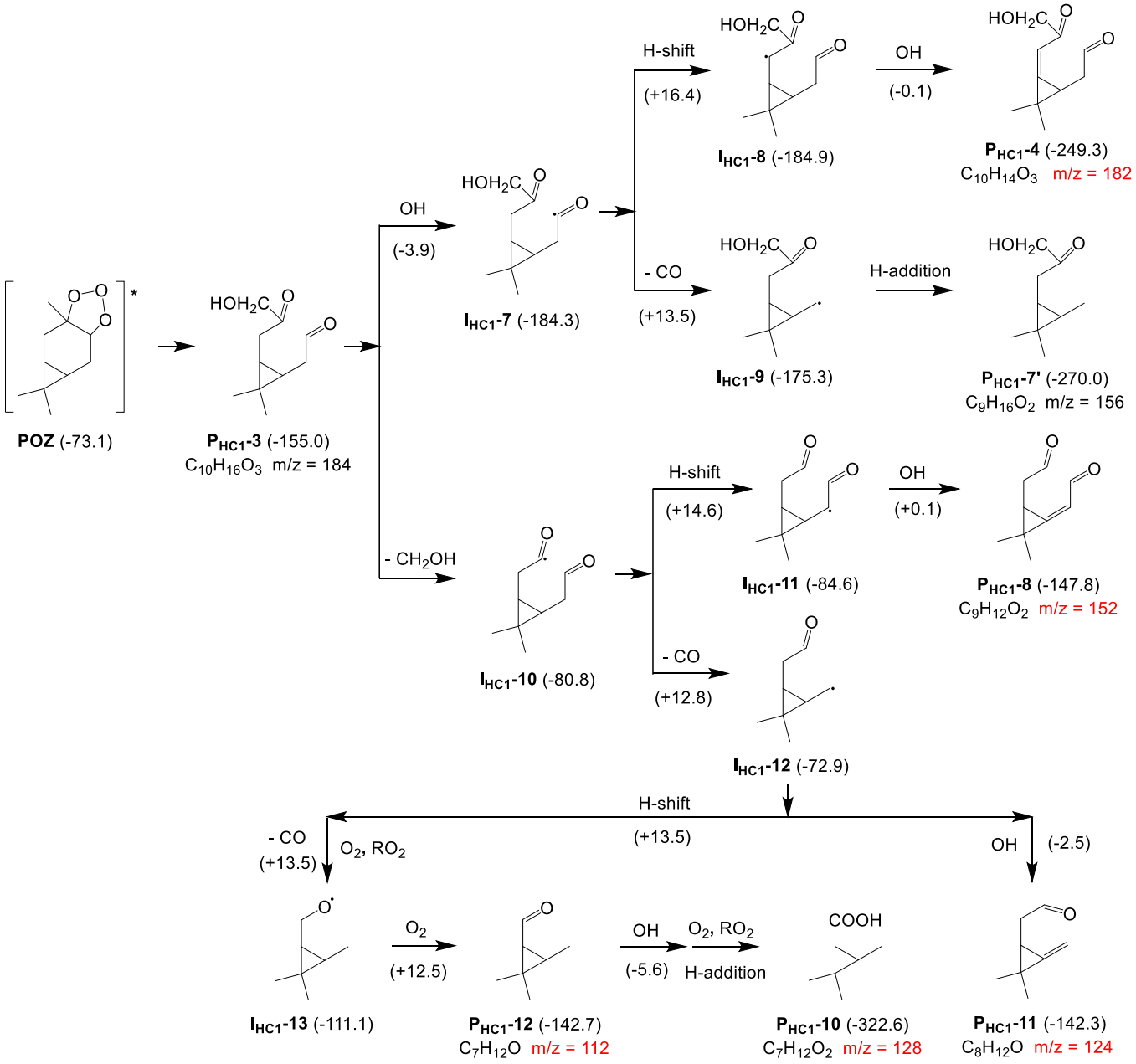

Fig. 4 – Possible formation mechanisms of newly-observed species P_{HC1}-*n* (*n* = 4, 7′, 8, 10, 11, 12) generated from the ozonolysis of Δ³-carene calculated at the ωB97XD/aug-cc-pVTZ//M06-2X/def2-TZVP level of theory. Relative energies are given in kcal/mol. The values in parentheses beside the arrows are the relative energies of transition states and reactants.

cess is exothermic by 31.9 kcal/mol. I_{HC2}–**2** reacts with O_2 and subsequently with HO_2 to form P_{HC2}–**3** (m/z = 214), which overall reaction is highly exothermic by 77.2 kcal/mol. The H-addition of I_{HC2}–**2** forms P_{HC2}–**5** (*m*/z = 182), which is even highly exothermic by 86.5 kcal/mol. **POZ** generated by the β-caryophyllene + O_3 reaction isomerizes to form I_{HC2}–**3**, which undergoes O_3 addition reaction to form I_{HC2}–**4**. The isomerization from I_{HC2}–**4** to I_{HC2}–**5** is exothermic by 23.4 kcal/mol with a barrier of 15.3 kcal/mol. I_{HC2}–**5** proceeds the hydrogen abstraction reaction of -CH- on the three-membered ring, releases CO_2, and then reacts with O_2 and RO_2 in sequence to form P_{HC2}–**5′** (m/z = 182), whose overall process is extremely exothermic by 257.2 kcal/mol. Similar to the I_{HC2}–**1** → I_{HC2}–**2** reaction, the P_{HC2}–**5′** → P_{HC2}–**6** reaction is facile and highly exothermic by 89.4 kcal/mol. P_{HC2}–**5′** could also react with O_3 to form I_{HC2}–**6**, which is then isomerized to form I_{HC2}–**7** with an exotherm of 13.8 kcal/mol and an isomerization barrier of 16.5 kcal/mol. I_{HC2}–**7** reacts with O_3 to produce P_{HC2}–**10** (m/z = 128), which is the fourth generation of ozonolysis product in this hypothesis.

The P_{HC2}-***m*** **(*m* = 7, 8, 9, 11, 12)** (m/z = 166, 152, 140, 126, 112) compounds have been proposed as the fragments (Appendix

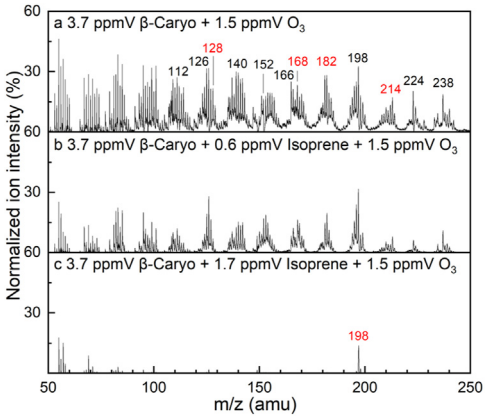

Fig. 5 – VUV-FEL photoionization mass spectra of the compounds generated from the ozonolysis of β-caryophyllene under different concentrations of isoprene. The compounds were ionized by the VUV-FEL at 118.0 nm. The newly-observed peaks are marked in red.

A Fig. S7). However, other fragment peaks were not detected (probably due to the rapid dissociation) (Du et al., 2023), and the relative proportions between the fragment peaks are different. Thus, these products are not definitely fragment peaks. Possible structures and formation pathways are shown in Appendix A Fig. S8.

2.3. *Hypothesis on the structures and formation paths for VOC-cross-product dimers*

In the two sets of Δ^3-carene + isoprene and β-caryophyllene + isoprene experiments, the change of mass spectral peaks of the products as a function of isoprene concentration is rather complicated. It is cumbersome to unambiguously clarify the sources and proportions for all these products because of their inherent complexity of the elementary reactions. However, the m/z = 224 peak in the Δ^3-carene + isoprene experiment and the m/z = 198 peak in the β-caryophyllene + isoprene experiment exhibits a relatively clear variation trend with independence of VOC mixtures, respectively. This suggests that the m/z = 224 and 198 peaks measured under mixed conditions might be mainly due to the representative VOC-cross products formed from the Δ^3-carene + isoprene and β-caryophyllene + isoprene experiments, respectively. The general bimolecular reactions based on literatures are listed in Appendix A Table S5. Based on the importance of RO_2 chemistry in the atmosphere (Orlando and Tyndall, 2012), the structures and formation paths of these two VOC-cross-product dimers (m/z = 224 and

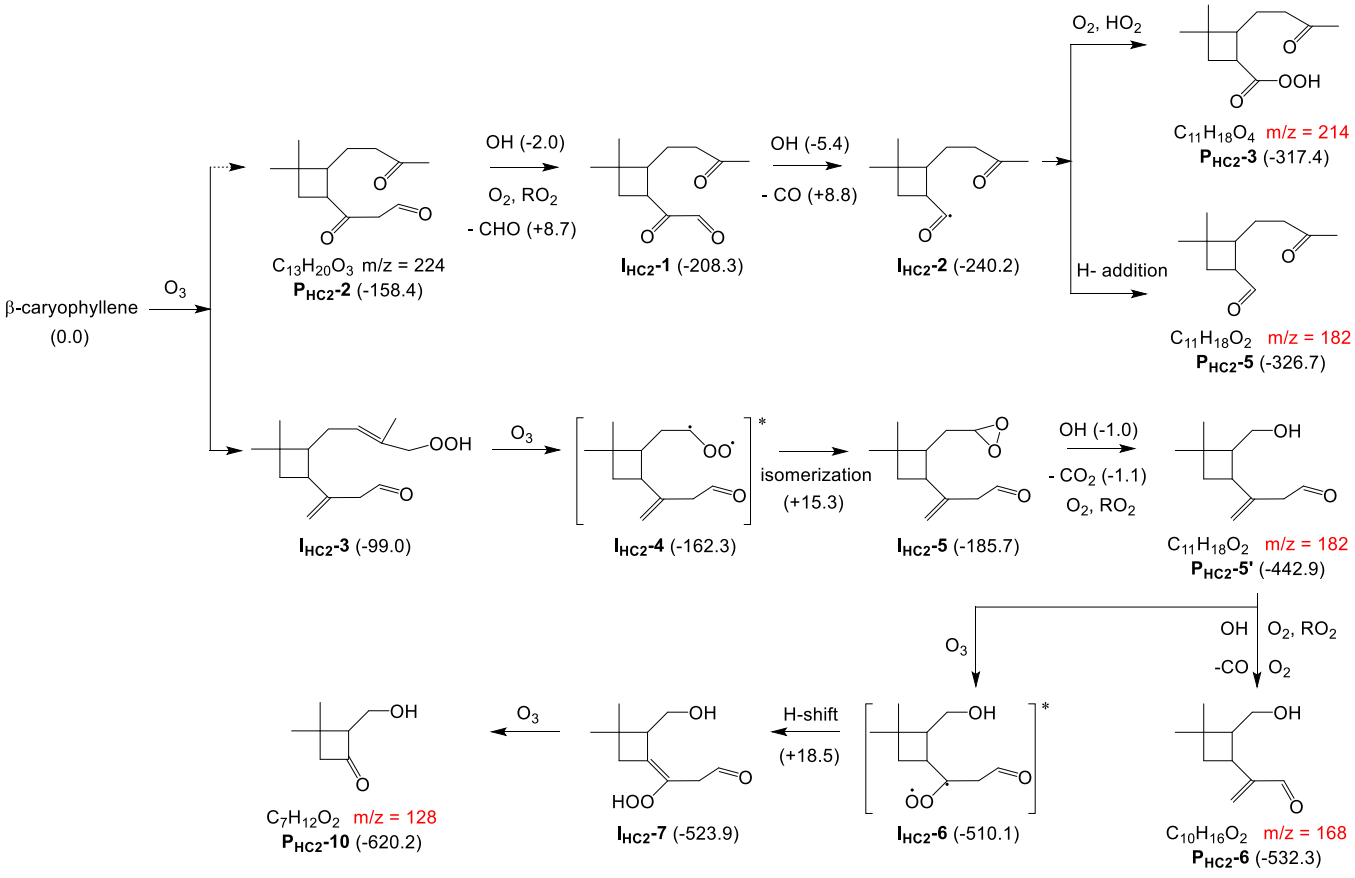

Fig. 6 – Possible formation mechanisms of newly-observed species P_{HC2}-*m* (*m* = 3, 5, 6, 10) generated from the ozonolysis of β-caryophyllene calculated at the ωB97XD/aug-cc-pVTZ//M06-2X/def2-TZVP level of theory. Relative energies are given in kcal/mol. The values in parentheses beside the arrows are the relative energies of transition states and reactants.

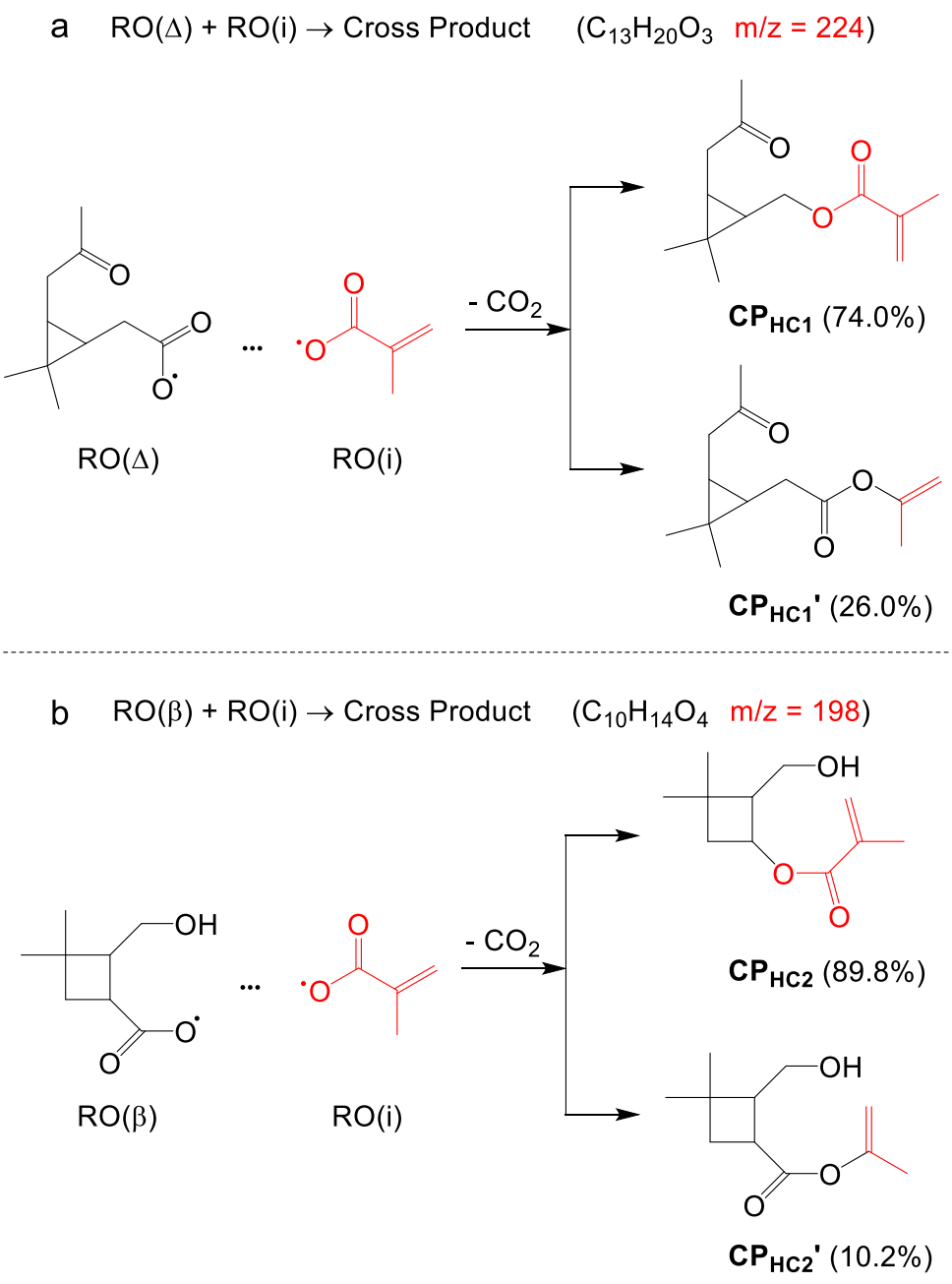

Fig. 7 – Hypothetical structures and formation mechanisms of cross products in the ozonolysis of isoprene with Δ^3-carene and isoprene with β-caryophyllene. RO(i), RO(Δ), and RO(β) are derived from isoprene, Δ^3-carene, and β-caryophyllene, respectively. Percentages in parentheses are relative values obtained from the reaction rate constant of RO dissociation CO_2.

198) are deduced from the cross reactions of RO_2. Typically, RO_2 undergoes chain termination via bimolecular reactions with NO, HO_2 and RO_2 (Vereecken et al., 2012). Previous studies have shown that the tetroxide (ROOOOR') intermediate formed by the reaction between different RO_2 radicals will rapidly decompose into a complex (RO…OR') and a free O_2 (Hasan et al., 2020). The complex (RO…OR') will undergo further dissociation or hydrogen migration to form RO + R'O or ROH + R''O, respectively (Orlando and Tyndall, 2012). More importantly, the complex can further form the well-known accretion product (ROOR) through intersystem crossing (ISC) (Hasan et al., 2021, 2020). However, the instability of ROOR has been identified in a recent study and RO with suitable structures can undergo extremely rapid C–C β scissions before RO recombination, resulting in ester products (Perakyla et al., 2023). These studies provide new insights into the formation of gas-phase accretion products in the process of aerosol formation.

Based on previous studies on the formation of accretion products centered around the RO complex, the structures and formation mechanisms of the m/z = 224 and 198 VOC-cross-product dimers are proposed in Fig. 7a and b, re-

spectively. RO(i), RO(Δ), and RO(β) are derived from isoprene, Δ^3-carene, and β-caryophyllene, respectively. Methacrolein (MACR) is one of the main ozonolysis products of isoprene (Galloway et al., 2011), which is autoxidized to RO_2(i) after H-abstraction reaction. RO_2(Δ) is generated from the autoxidation of I_{HC1}–3. As shown in Fig. 7a, after dissociation of CO_2 from RO(Δ)…OR(i), subsequent reactions can lead to the formation of either R'(Δ)…OR(i) or RO(Δ)…R'(i), resulting in the formation of cross product (CP) of **CP_{HC1}** or **CP_{HC1}'**, respectively. The calculated results (Appendix A Fig. S10a) show that the energy of the singlet **CP_{HC1}** and **CP_{HC1}'** is about 76.5 kcal/mol lower than that of the triplet state, indicating that ^{3}(RO(Δ)…R'(i)) or ^{3}(R'(Δ)…OR(i)) is easy to undergo ISC to form a more stable closed-shell product. Before the recombination of RO(i) and RO(Δ), the dissociation rate constant of CO_2 by RO(i) and RO(Δ) is 4.32×10^{11} sec^{-1} and 1.23×10^{12} sec^{-1}, respectively. Considering the involvement of other isomerization processes of complex RO(Δ)…OR(i), the rather slow intramolecular H-shift reaction, with a rate on the order of 1×10^9 sec^{-1} or below, competes weakly with the dissociation process of CO_2 from RO. In addition, the dissociation of the ^{3}(RO(Δ)…OR(i)) complex to RO(Δ) and RO(i) is slightly endothermic by 7.1 kcal/mol, which may compete strongly with the dissociation of RO. However, the dissociation of the ^{3}(RO(i)…OR(Δ)) complex into ^{3}(R'(Δ)…OR(i)) + CO_2 or ^{3}(RO(Δ)…R'(i)) + CO_2 is exothermic by 19.5 kcal/mol and 7.6 kcal/mol, respectively, indicating that the process of releasing CO_2 from the complex is more thermodynamically favorable. In conclusion, RO(i) and RO(Δ) compete more significantly for the dissociation of CO_2 for the formation of VOC-cross-product dimers. Assuming that the concentration of RO_2(i) and RO_2(Δ) is not taken into account, the relative proportion (%) of **CP_{HC1}** and **CP_{HC1}'** can be determined based on the dissociation rate of CO_2. Similarly, the structures of VOC-cross-product dimers derived from RO(β)…OR (i) are shown in Fig. 7b, and the formation pathway of RO_2(β) is shown in Appendix A Fig. S9. The dissociation rate constant of CO_2 by RO(β) is 3.80×10^{12} sec^{-1}, and the relative proportions of **CP_{HC2}** and **CP_{HC2}'** are 89.8% and 10.2%, respectively. The associated energy information is shown in Appendix A Fig. S10b.

3. Conclusions and atmospheric implications

In this study, two series of double precursor experiments were carried out under O_3 conditions. Based on the mutual competition of precursor VOCs, different mixed concentrations of isoprene can significantly regulate the ozonolysis of Δ^3-carene and β-caryophyllene to form SOA. With the increase of the mixing amount of isoprene, a fluctuation suppression trend is observed in the isoprene + Δ^3-carene experiment, whereas a monotonous suppression trend is found in the isoprene + β-caryophyllene experiment. Such different suppression effects of isoprene could be closely related to the carbon content of the precursor, for which the generation of products with lower volatility plays a key role in the regulation of the SOA formation. The decreased suppression effect of isoprene on Δ^3-carene ozonolysis may be attributed to the increased generation of C_{15} dimers that promote the SOA formation. The more obvious suppression effect of isoprene on β-caryophyllene ozonolysis may be due to the reduction of oxidized β-caryophyllene, resulting in a decrease of the production of C_{20} dimers. This provides fundamental insights into the divergent outcomes resulted from the competitive reactions between the different VOC precursors under O_3 conditions. Furthermore, to improve SOA simulations and to develop strategies for controlling particles pollution, the competition between VOCs and primary/secondary oxidants needs to be considered in more details. It has been shown that the isoprene emitted at dusk could persist until the night (Brown et al., 2009; Stroud et al., 2002). For the cities downwind of isoprene-emitting forests, the nighttime isoprene chemistry may have a critical impact on the ozone air quality and photochemistry (Millet et al., 2016).

In the courtesy of high photoionization efficiency of tunable VUV-FEL, several new products formed from the ozonolysis of Δ^3-carene and β-caryophyllene are observed, which advance our understanding of the related oxidation product categories. Based on the speculation of the formation of VOC-cross-product dimers, a new path for the formation of stable accretion products derived from RO…OR complex is proposed: R(CO)O would quickly decompose CO_2 to form R' before two R(CO)O recombining, and R(CO)O…R' reacts to form a more stable ester product. The dissociations of CO_2 by R(CO)O and R'(CO)O are highly competitive, resulting in the formation of dimers with variable structures. It is inferred that a large number of ester or ether products would be formed by cross-reaction of RO_2 derived from the same or different precursors in a similar manner. The stability of esters compared to peroxides makes this new pathway crucial in the formation of long-lived, low-volatility accretion products for atmospheric aerosol formation. Moreover, a meticulous analysis of the interactions among reaction intermediates is also important for precise evaluation of the physical and chemical characteristics of SOA. Note that the concentrations of VOCs utilized in this work are two/three orders of magnitude higher than the atmospheric concentrations, for which the new particle formation might be different from the atmospheric SOA. It was found that recent laboratory and field studies at high concentrations of VOCs and anthropogenic pollutants have contributed to understand the complicated mechanisms of SOA formation at various conditions, especially nearby the emission origins (Boge et al., 2006; Jaoui et al., 2021; Kleindienst et al., 2006, 2007; Lin et al., 2013; Surratt et al., 2007). The improvement of VUV-FEL photoionization aerosol mass spectrometric experiments at the concentrations of reactants close to atmospheric conditions is on the way.

Declaration of Competing Interest

The authors have no conflicts to disclose.

Acknowledgments

This work was supported by the National Natural Science Foundation of China (Nos. 92361302, 22125303, 92061203, and 22288201), the National Key Research and Development Program of China (No. 2021YFA1400501), the Innovation Program

for Quantum Science and Technology (No. 2021ZD0303304), Dalian Institute of Chemical Physics (No. DICP DCLS201702), and Chinese Academy of Sciences (No. GJJSTD20220001). The authors gratefully acknowledge the Dalian Coherent Light Source (DCLS) for support and assistance.

Appendix A Supplementary data

Supplementary material associated with this article can be found in the online version at doi:10.1016/j.jes.2023.11.024.

References

Ahlberg, E., Falk, J., Eriksson, A., Holst, T., Brune, W.H., Kristensson, A., et al., 2017. Secondary organic aerosol from VOC mixtures in an oxidation flow reactor. Atmos. Environ. 161, 210–220.

Amaladhasan, D.A., Heyn, C., Hoyle, C.R., El Haddad, I., Elser, M., Pieber, S.M., et al., 2022. Modelling the gas-particle partitioning and water uptake of isoprene-derived secondary organic aerosol at high and low relative humidity. Atmos. Chem. Phys. 22, 215–244.

Appel, K.W., Napelenok, S.L., Foley, K.M., Pye, H.O.T., Hogrefe, C., Luecken, D.J., et al., 2017. Description and evaluation of the community multiscale air quality (CMAQ) modeling system version 5.1. Geosci. Model. Dev. 10, 1703–1732.

Atkinson, R., 2000. Atmospheric chemistry of VOCs and NO_X. Atmos. Environ. 34, 2063–2101.

Atkinson, R., Arey, J., 2003. Gas-phase tropospheric chemistry of biogenic volatile organic compounds: A review. Atmos. Environ. 37, S197–S219.

Bao, J.L., Truhlar, D.G., 2017. Variational transition state theory: Theoretical framework and recent developments. Chem. Soc. Rev. 46, 7548–7596.

Boge, O., Miao, Y., Plewka, A., Herrmann, H., 2006. Formation of secondary organic particle phase compounds from isoprene gas-phase oxidation products: An aerosol chamber and field study. Atmos. Environ. 40, 2501–2509.

Bonn, B., Moortgat, G.K., 2002. New particle formation during alpha- and beta-pinene oxidation by O_3, OH and NO_3, and the influence of water vapour: Particle size distribution studies. Atmos. Chem. Phys. 2, 183–196.

Brauer, M., Freedman, G., Frostad, J., van Donkelaar, A., Martin, R.V., Dentener, F., et al., 2016. Ambient air pollution exposure estimation for the global burden of disease 2013. Environ. Sci. Technol. 50, 79–88.

Brown, S.S., deGouw, J.A., Warneke, C., Ryerson, T.B., Dube, W.P., Atlas, E., et al., 2009. Nocturnal isoprene oxidation over the Northeast United States in summer and its impact on reactive nitrogen partitioning and secondary organic aerosol. Atmos. Chem. Phys. 9, 3027–3042.

Canneaux, S., Bohr, F., Henon, E., 2014. KiSThelP: A program to predict thermodynamic properties and rate constants from quantum chemistry results. J. Comput. Chem. 35, 82–93.

Chen, T., Zhang, P., Chu, B., Ma, Q., Ge, Y., Liu, J., et al., 2022. Secondary organic aerosol formation from mixed volatile organic compounds: effect of RO_2 chemistry and precursor concentration. NPJ Clim. Atmos. Sci. 5, 95.

Ciccioli, P., Brancaleoni, E., Frattoni, M., Di Palo, V., Valentini, R., Tirone, G., et al., 1999. Emission of reactive terpene compounds from orange orchards and their removal by within-canopy processes. J. Geophys. Res. Atmos. 104, 8077–8094.

Dada, L., Stolzenburg, D., Simon, M., Fischer, L., Heinritzi, M., Wang, M., et al., 2023. Role of sesquiterpenes in biogenic new particle formation. Sci. Adv. 9, eadi5297.

Du, L., Xu, L., Li, K., George, C., Ge, M., 2023. NH_3 weakens the enhancing effect of SO_2 on biogenic secondary organic aerosol formation. Environ. Sci. Technol. Lett. 10, 145–151.

Ehn, M., Thornton, J.A., Kleist, E., Sipila, M., Junninen, H., Pullinen, I., et al., 2014. A large source of low-volatility secondary organic aerosol. Nature 506, 476–479.

Faiola, C.L., Buchholz, A., Kari, E., Yli-Pirila, P., Holopainen, J.K., Kivimaenpaa, M., et al., 2018. Terpene composition complexity controls secondary organic aerosol yields from scots pine volatile emissions. Sci. Rep. UK 8, 3053.

Frisch, M.J., Trucks, G.W., Schlegel, H.B., Scuseria, G.E., Robb, M.A., Cheeseman, J.R., et al., 2016. Gaussian 16. Gaussian, Inc., Wallingford, CT.

Fuchs, H., Acir, I.H., Bohn, B., Brauers, T., Dorn, H.P., Haeseler, R., et al., 2014. OH regeneration from methacrolein oxidation investigated in the atmosphere simulation chamber SAPHIR. Atmos. Chem. Phys. 14, 7895–7908.

Galloway, M.M., Huisman, A.J., Yee, L.D., Chan, A.W.H., Loza, C.L., Seinfeld, J.H., et al., 2011. Yields of oxidized volatile organic compounds during the OH radical initiated oxidation of isoprene, methyl vinyl ketone, and methacrolein under high-NO_x conditions. Atmos. Chem. Phys. 11, 10779–10790.

Gao, S., Ng, N.L., Keywood, M., Varutbangkul, V., Bahreini, R., Nenes, A., et al., 2004. Particle phase acidity and oligomer formation in secondary organic aerosol. Environ. Sci. Technol. 38, 6582–6589.

Geron, C.D., Arnts, R.R., 2010. Seasonal monoterpene and sesquiterpene emissions from Pinus taeda and Pinus virginiana. Atmos. Environ. 44, 4240–4251.

Guenther, A.B., Jiang, X., Heald, C.L., Sakulyanontvittaya, T., Duhl, T., Emmons, L.K., et al., 2012. The model of emissions of gases and aerosols from nature version 2.1 (MEGAN2.1): an extended and updated framework for modeling biogenic emissions. Geosci. Model. Dev. 5, 1471–1492.

Hallquist, M., Wenger, J.C., Baltensperger, U., Rudich, Y., Simpson, D., Claeys, M., et al., 2009. The formation, properties and impact of secondary organic aerosol: current and emerging issues. Atmos. Chem. Phys. 9, 5155–5236.

Hamilton, J.F., Lewis, A.C., Reynolds, J.C., Carpenter, L.J., Lubben, A., 2006. Investigating the composition of organic aerosol resulting from cyclohexene ozonolysis: Low molecular weight and heterogeneous reaction products. Atmos. Chem. Phys. 6, 4973–4984.

Hantschke, L., Novelli, A., Bohn, B., Cho, C., Reimer, D., Rohrer, F., et al., 2021. Atmospheric photooxidation and ozonolysis of Δ^3-carene and 3-caronaldehyde: Rate constants and product yields. Atmos. Chem. Phys. 21, 12665–12685.

Hasan, G., Valiev, R.R., Salo, V.-T., Kurten, T., 2021. Computational investigation of the formation of peroxide (ROOR) accretion products in the OH- and NO_3-initiated oxidation of alpha-pinene. J. Phys. Chem. A 125, 10632–10639.

Hasan, G., Salo, V.-T., Valiev, R.R., Kubecka, J., Kurten, T., 2020. Comparing reaction routes for ^{3}(RO···OR') intermediates formed in peroxy radical self- and cross-reactions. J. Phys. Chem. A 124, 8305–8320.

Heinritzi, M., Dada, L., Simon, M., Stolzenburg, D., Wagner, A.C., Fischer, L., et al., 2020. Molecular understanding of the suppression of new-particle formation by isoprene. Atmos. Chem. Phys. 20, 11809–11821.

Jaoui, M., Piletic, I.R., Szmigielski, R., Rudzinski, K.J., Lewandowski, M., Riedel, T.P., et al., 2021. Rapid production of highly oxidized molecules in isoprene aerosol via peroxy and alkoxy radical isomerization pathways in low and high NOx environments: Combined laboratory, computational and field studies. Sci. Total. Environ. 775.

Kanawade, V.P., Jobson, B.T., Guenther, A.B., Erupe, M.E., Pressley, S.N., Tripathi, S.N., et al., 2011. Isoprene suppression of new particle formation in a mixed deciduous forest. Atmos. Chem. Phys. 11, 6013–6027.
Kleindienst, T.E., Edney, E.O., Lewandowski, M., Offenberg, J.H., Jaoui, M., 2006. Secondary organic carbon and aerosol yields from the irradiations of isoprene and alpha-pinene in the presence of NO_x and SO_2. Environ. Sci. Technol. 40, 3807–3812.
Kleindienst, T.E., Jaoui, M., Lewandowski, M., Offenberg, J.H., Lewis, C.W., Bhave, P.V., et al., 2007. Estimates of the contributions of biogenic and anthropogenic hydrocarbons to secondary organic aerosol at a southeastern US location. Atmos. Environ. 41, 8288–8300.
Koch, S., Winterhalter, R., Uherek, E., Kolloff, A., Neeb, P., Moortgat, G.K., 2000. Formation of new particles in the gas-phase ozonolysis of monoterpenes. Atmos. Environ. 34, 4031–4042.
Krechmer, J.E., Day, D.A., Jimenez, J.L., 2020. Always lost but never forgotten: gas-phase wall losses are important in all teflon environmental chambers. Environ. Sci. Technol. 54, 12890–12897.
Lee, S.H., Uin, J., Guenther, A.B., de Gouw, J.A., Yu, F., Nadykto, A.B., et al., 2016. Isoprene suppression of new particle formation: Potential mechanisms and implications. J. Geophys. Res. Atmos. 121, 14621–14635.
Lester, M.I., Klippenstein, S.J., 2018. Unimolecular decay of criegee intermediates to OH radical products: Prompt and thermal decay processes. Acc. Chem. Res. 51, 978–985.
Lewis, A.C., 2018. The changing face of urban air pollution. Science 359, 744–745.
Li, J., Li, H., Li, K., Chen, Y., Zhang, H., Zhang, X., et al., 2021. Enhanced secondary organic aerosol formation from the photo-oxidation of mixed anthropogenic volatile organic compounds. Atmos. Chem. Phys. 21, 7773–7789.
Li, K., Zhang, X., Zhao, B., Bloss, W.J., Lin, C., White, S., et al., 2022. Suppression of anthropogenic secondary organic aerosol formation by isoprene. NPJ Clim. Atmos. Sci. 5, 12.
Lin, Y.-H., Zhang, H., Pye, H.O.T., Zhang, Z., Marth, W.J., Park, S., et al., 2013. Epoxide as a precursor to secondary organic aerosol formation from isoprene photooxidation in the presence of nitrogen oxides. Proc. Natl. Acad. Sci. U. S. A. 110, 6718–6723.
Liu, Y., Brito, J., Dorris, M.R., Rivera-Rios, J.C., Seco, R., Bates, K.H., et al., 2016. Isoprene photochemistry over the Amazon rainforest. Proc. Natl. Acad. Sci. U. S. A. 113, 6125–6130.
Lu, T. (2023). Molcus program, Version 1.9.9.9, http://www.keinsci.com/research/molclus.html. Accessed June 4, 2023.
Ma, Y., Porter, R.A., Chappell, D., Russell, A.T., Marston, G., 2009. Mechanisms for the formation of organic acids in the gas-phase ozonolysis of 3-carene. Phys. Chem. Chem. Phys. 11, 4184–4197.
McFiggans, G., Mentel, T.F., Wildt, J., Pullinen, I., Kang, S., Kleist, E., et al., 2019. Secondary organic aerosol reduced by mixture of atmospheric vapours. Nature 565, 587–593.
Millet, D.B., Baasandorj, M., Hu, L., Mitroo, D., Turner, J., Williams, B.J., 2016. Nighttime chemistry and morning isoprene can drive urban ozone downwind of a major deciduous forest. Environ. Sci. Technol. 50, 4335–4342.
Mueller, L., Reinnig, M.C., Warnke, J., Hoffmann, T., 2008. Unambiguous identification of esters as oligomers in secondary organic aerosol formed from cyclohexene and cyclohexene/alpha-pinene ozonolysis. Atmos. Chem. Phys. 8, 1423–1433.
Ng, N.L., Chhabra, P.S., Chan, A.W.H., Surratt, J.D., Kroll, J.H., Kwan, A.J., et al., 2007. Effect of NOx level on secondary organic aerosol (SOA) formation from the photooxidation of terpenes. Atmos. Chem. Phys. 7, 5159–5174.
Orlando, J.J., Tyndall, G.S., 2012. Laboratory studies of organic peroxy radical chemistry: an overview with emphasis on recent issues of atmospheric significance. Chem. Soc. Rev. 41, 6294–6317.
Pathak, R.K., Stanier, C.O., Donahue, N.M., Pandis, S.N., 2007. Ozonolysis of alpha-pinene at atmospherically relevant concentrations: temperature dependence of aerosol mass fractions (yields). J. Geophys. Res. Atmos. 112.
Perakyla, O., Berndt, T., Franzon, L., Hasan, G., Meder, M., Valiev, R.R., et al., 2023. Large gas-phase source of esters and other accretion products in the atmosphere. J. Am. Chem. Soc. 145, 7780–7790.
Salo, V.-T., Valiev, R., Lehtola, S., Kurten, T., 2022. Gas-phase peroxyl radical recombination reactions: a computational study of formation and decomposition of tetroxides. J. Phys. Chem. A 126, 4046–4056.
Shiraiwa, M., Ueda, K., Pozzer, A., Lammel, G., Kampf, C.J., Fushimi, A., et al., 2017. Aerosol health effects from molecular to global scales. Environ. Sci. Technol. 51, 13545–13567.
Shrivastava, M., Andreae, M.O., Artaxo, P., Barbosa, H.M.J., Berg, L.K., Brito, J., et al., 2019. Urban pollution greatly enhances formation of natural aerosols over the Amazon rainforest. Nat. Commun. 10, 1046.
Stroud, C.A., Roberts, J.M., Williams, E.J., Hereid, D., Angevine, W.M., Fehsenfeld, F.C., et al., 2002. Nighttime isoprene trends at an urban forested site during the 1999 Southern Oxidant Study. J. Geophys. Res. Atmos. 107.
Surratt, J.D., Lewandowski, M., Offenberg, J.H., Jaoui, M., Kleindienst, T.E., Edney, E.O., et al., 2007. Effect of acidity on secondary organic aerosol formation from isoprene. Environ. Sci. Technol. 41, 5363–5369.
Takeuchi, M., Berkemeier, T., Eris, G., Ng, N.L., 2022. Non-linear effects of secondary organic aerosol formation and properties in multi-precursor systems. Nat. Commun. 13, 7883.
Thomsen, D., Thomsen, L.D., Iversen, E.M., Bjorgvinsdottir, T.N., Vinther, S.F., Skonager, J.T., et al., 2022. Ozonolysis of alpha-pinene and delta 3-carene mixtures: Formation of dimers with two precursors. Environ. Sci. Technol. 56, 16643–16651.
Tolocka, M.P., Jang, M., Ginter, J.M., Cox, F.J., Kamens, R.M., Johnston, M.V., 2004. Formation of oligomers in secondary organic aerosol. Environ. Sci. Technol. 38, 1428–1434.
Vereecken, L., Harder, H., Novelli, A., 2012. The reaction of Criegee intermediates with NO, RO_2, and SO_2, and their fate in the atmosphere. Phys. Chem. Chem. Phys. 14, 14682–14695.
Wennberg, P.O., Bates, K.H., Crounse, J.D., Dodson, L.G., McVay, R.C., Mertens, L.A., et al., 2018. Gas-phase reactions of isoprene and its major oxidation products. Chem. Rev. 118, 3337–3390.
Wimmer, D., Mazon, S.B., Manninen, H.E., Kangasluoma, J., Franchin, A., Nieminen, T., et al., 2018. Ground-based observation of clusters and nucleation-mode particles in the Amazon. Atmos. Chem. Phys. 18, 13245–13264.
Winterhalter, R., Herrmann, F., Kanawati, B., Nguyen, T.L., Peeters, J., Vereecken, L., et al., 2009. The gas-phase ozonolysis of beta-caryophyllene ($C_{15}H_{24}$). Part I: An experimental study. Phys. Chem. Chem. Phys. 11, 4152–4172.
Xu, L., Guo, H., Boyd, C.M., Klein, M., Bougiatioti, A., Cerully, K.M., et al., 2015. Effects of anthropogenic emissions on aerosol formation from isoprene and monoterpenes in the southeastern United States. Proc. Natl. Acad. Sci. U. S. A. 112, 37–42.
Yasmeen, F., Vermeylen, R., Szmigielski, R., Iinuma, Y., Boege, O., Herrmann, H., et al., 2010. Terpenylic acid and related compounds: precursors for dimers in secondary organic aerosol from the ozonolysis of alpha- and beta-pinene. Atmos. Chem. Phys. 10, 9383–9392.
Yu, J.Z., Flagan, R.C., Seinfeld, J.H., 1998. Identification of products containing -COOH, -OH, and -C=O in atmospheric oxidation of hydrocarbons. Environ. Sci. Technol. 32, 2357–2370.

Yu, J.Z., Cocker, D.R., Griffin, R.J., Flagan, R.C., Seinfeld, J.H., 1999. Gas-phase ozone oxidation of monoterpenes: Gaseous and particulate products. J. Atmos. Chem. 34, 207–258.
Zang, X., Zhang, Z., Jiang, S., Zhao, Y., Wang, T., Wang, C., et al., 2022. Aerosol mass spectrometry of neutral species based on a tunable vacuum ultraviolet free electron laser. Phys. Chem. Chem. Phys. 24, 16484–16492.
Zhang, D., Zhang, R.Y., 2002. Mechanism of OH formation from ozonolysis of isoprene: a quantum-chemical study. J. Am. Chem. Soc. 124, 2692–2703.
Zhang, D., Lei, W.F., Zhang, R.Y., 2002. Mechanism of OH formation from ozonolysis of isoprene: kinetics and product yields. Chem. Phys. Lett. 358, 171–179.
Zhang, R.Y., 2010. Getting to the critical nucleus of aerosol formation. Science 328, 1366–1367.
Zhang, R.Y., Suh, I., Lei, W., Clinkenbeard, A.D., North, S.W., 2000. Kinetic studies of OH-initiated reactions of isoprene. J. Geophys. Res. Atmos. 105, 24627–24635.
Zhang, R.Y., Suh, I., Zhao, J., Zhang, D., Fortner, E.C., Tie, X.X., et al., 2004. Atmospheric new particle formation enhanced by organic acids. Science 304, 1487–1490.
Zhang, X., Cappa, C.D., Jathar, S.H., McVay, R.C., Ensberg, J.J., Kleeman, M.J., et al., 2014. Influence of vapor wall loss in laboratory chambers on yields of secondary organic aerosol. Proc. Natl. Acad. Sci. U. S. A. 111, 5802–5807.